Global Biogeochemical Cycles

RESEARCH ARTICLE
10.1029/2018GB005887

Key Points:
- New quantitative relationships between oxygen and nitrous oxide production are derived from direct measurements in low-oxygen oceans
- The presence of oxygen reduces nitrous oxide production via nitrification and denitrification
- The latest biogeochemical model incorporating the field measurements and relationships provides new estimate of global marine nitrous oxide flux

Supporting Information:
- Supporting Information S1
- Data Set S1

Correspondence to:
Q. Ji,
qji@alumni.princeton.edu

Citation:
Ji, Q., Buitenhuis, E., Suntharalingam, P., Sarmiento, J. L., & Ward, B. B. (2018). Global nitrous oxide production determined by oxygen sensitivity of nitrification and denitrification. *Global Biogeochemical Cycles*, *32*, 1790–1802. https://doi.org/10.1029/2018GB005887

Received 16 JAN 2018
Accepted 21 NOV 2018
Accepted article online 23 NOV 2018
Published online 12 DEC 2018

Global Nitrous Oxide Production Determined by Oxygen Sensitivity of Nitrification and Denitrification

Qixing Ji[1,2], Erik Buitenhuis[3], Parvadha Suntharalingam[3], Jorge L. Sarmiento[4], and Bess B. Ward[1]

[1]Department of Geosciences, Princeton University, Princeton, NJ, USA, [2]Now at Helmholtz Centre for Ocean Research Kiel, Kiel, Germany, [3]School of Environmental Science, University of East Anglia, Norfolk, UK, [4]Program in Atmospheric and Oceanic Sciences, Princeton University, Princeton, NJ, USA

Abstract The ocean is estimated to contribute up to ~20% of global fluxes of atmospheric nitrous oxide (N_2O), an important greenhouse gas and ozone depletion agent. Marine oxygen minimum zones contribute disproportionately to this flux. To further understand the partition of nitrification and denitrification and their environmental controls on marine N_2O fluxes, we report new relationships between oxygen concentration and rates of N_2O production from nitrification and denitrification directly measured with ^{15}N tracers in the Eastern Tropical Pacific. Highest N_2O production rates occurred near the oxic-anoxic interface, where there is strong potential for N_2O efflux to the atmosphere. The dominant N_2O source in oxygen minimum zones was nitrate reduction, the rates of which were 1 to 2 orders of magnitude higher than those of ammonium oxidation. The presence of oxygen significantly inhibited the production of N_2O from both nitrification and denitrification. These experimental data provide new constraints to a multicomponent global ocean biogeochemical model, which yielded annual oceanic N_2O efflux of 1.7–4.4 Tg-N (median 2.8 Tg-N, 1 Tg = 10^{12} g), with denitrification contributing 20% to the oceanic flux. Thus, denitrification should be viewed as a net N_2O production pathway in the marine environment.

1. Introduction

The unprecedented rate of increase in atmospheric nitrous oxide (N_2O) concentration since the Industrial Revolution (Blasing, 2016) is alarming because N_2O is a strong greenhouse gas and, following the successful mitigation of halocarbons, will be the most important ozone depletion agent by the end of the 21st century (Ravishankara et al., 2009). N_2O from soil, coastal waters, and the open ocean is emitted into the troposphere, where N_2O is chemically inert, resulting in the pronounced increase of N_2O burden. The average lifetime of N_2O in the atmosphere is estimated to be more than 100 years (Prather et al., 2012); photolytic destruction in the stratosphere is the major sink. Intense N_2O emissions in the open ocean occur in upwelling regions where oxygen minimum zones (OMZs) are located (Codispoti, 2010). OMZs are characterized by sharp oxygen (O_2) gradients (oxycline strength >2.5 $\mu mol \cdot L^{-1} \cdot m^{-1}$) overlying an anoxic layer of hundreds of meters in depth. Extreme N_2O supersaturation with respect to the atmosphere occurs in the oxycline, indicating active N_2O production and the potential for efflux to the atmosphere (Codispoti & Christensen, 1985; Elkins et al., 1978; Law & Owens, 1990). Although the OMZs occupy $<1\%$ of the ocean volume (Codispoti et al., 2001), they potentially contribute up to 50% of marine N_2O efflux (Codispoti, 2010). The Intergovernmental Panel on Climate Change reports that the ocean contributes 3.8 Tg-N/year (1 Tg = 10^{12} g), ~21% of the total N_2O emissions (Ciais et al., 2013). However, incomplete understanding of marine N_2O production pathways and their sensitivities to environmental factors resulted in large uncertainties of current N_2O emission estimates (1.8–9.4 Tg-N/year) and limited our ability to predict future N_2O emission under the changing ocean and climate (Battaglia & Joos, 2018; Landolfi et al., 2017).

Biological N_2O production in the ocean is attributed to ammonium (NH_4^+) oxidation, nitrite (NO_2^-) reduction, and nitrate (NO_3^-) reduction (Figure 1). During aerobic NH_4^+ oxidation to NO_2^-, the first step in nitrification (by both bacteria and archaea), N_2O is emitted as a byproduct, with higher N_2O yield (the molar nitrogen ratio of N_2O to NO_2^- production) at lower O_2 conditions (Goreau et al., 1980; Löscher et al., 2012). Under low O_2 and anoxic conditions, NO_3^- and NO_2^- can be reduced to N_2O through stepwise conventional denitrification ($NO_3^- \rightarrow NO_2^- \rightarrow NO \rightarrow N_2O$), with organic matter as the electron donor. Nitrite reduction, which occurs in O_2 conditions from fully saturated to functional anoxia (Frame & Casciotti, 2010), is mediated by both nitrifiers (Poth &

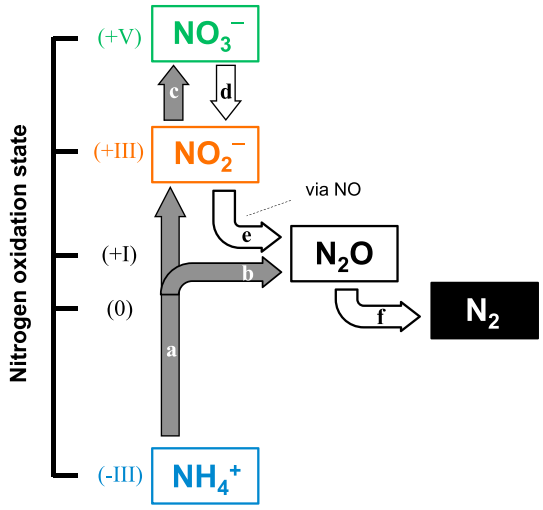

Figure 1. Nitrogen transformations related to N_2O production and consumption in marine environments. (a) Ammonium (NH_4^+) oxidation to nitrite (NO_2^-). (b) NH_4^+ oxidation to N_2O. (c) NO_2^- oxidation to nitrate (NO_3^-). (d) NO_3^- reduction to NO_2^-. (e) NO_2^- reduction to N_2O via nitric oxide (NO). (f) N_2O reduction to N_2. Filled arrows (reactions a–c) represent oxidative pathways, requiring molecular oxygen as terminal electron acceptor. Open arrows (reactions d–f) represent reductive pathways requiring organic matter as the electron donor. In the main text, N_2O production from nitrification includes pathways (b) and (a) coupled with (e); N_2O production from denitrification includes pathways (e) and (d) coupled with (e).

Focht, 1985) and denitrifiers (Cohen & Gordon, 1978). "Nitrifier denitrification" refers to NO_2^- reduction to N_2O in oxygenated water column where conventional denitrification is insignificant (Wilson et al., 2014). In the OMZs, the sharp O_2 gradient provides niches for both nitrifying and denitrifying organisms to enable N_2O production from both nitrification and denitrification (Codispoti & Christensen, 1985). In this study, "nitrification" refers to NH_4^+ oxidation, whereas "denitrification" refers to NO_3^- and NO_2^- reduction. At present, distinguishing nitrifier denitrification from conventional denitrification (i.e., both can conduct NO_2^- reduction to N_2O) in natural environments is difficult due to the lack of reliable methodology.

Nitrification is regarded as the main pathway of global oceanic N_2O production because denitrification is mainly restricted to OMZs and because N_2O consumption is assumed to dominate over N_2O production by denitrification in the OMZs (Codispoti, 2010; Freing et al., 2012). This notion was challenged by recent observations and model analysis (Babbin et al., 2015; Bourbonnais et al., 2017; Ji et al., 2015), which suggested high rates of N_2O production from NO_3^- reduction in the OMZs. Lacking reliable quantification of nitrogen cycling processes in OMZs, previous biogeochemical models predominantly employed simple parameterizations representing N_2O production derived from limited culture analyses and in situ measurements, and model analysis of the relative contribution of N_2O production from denitrification and nitrification to the total oceanic flux is uncertain (Battaglia & Joos, 2018; Suntharalingam et al., 2012).

We applied nitrogen stable isotope (^{15}N) incubation experiments to directly measure rates and pathways of N_2O production in the OMZs of the Eastern Tropical South and North Pacific (ETSP and ETNP). To evaluate control of N_2O production by oxygen, we derived quantitative relationships between oxygen concentration and N_2O production from NH_4^+ oxidation, NO_2^-, and NO_3^- reduction. The rate distribution and O_2 relationships were incorporated into a multicomponent ocean biogeochemistry and ecosystem model to estimate global oceanic N_2O fluxes and to partition the contributions of the nitrification and denitrification pathways.

2. Methods

2.1. Shipboard Sampling

Shipboard sampling and incubation experiments were carried out on the R/V *Atlantis* during January 2015 (Cruise ID: AT26-26); and R/V *Ronald H. Brown* during April 2016 (Cruise ID: RB1603). Samples were collected from the North (15–20°N) and South Pacific (10–20°S) coastal upwelling zones off the coast of Mexico and Peru (Figure 2). Stations were chosen to represent coastal environment (<185.2 km from the coast) and open ocean environment (>370.4 km from the coast). Water was collected in 12-L Niskin bottles mounted on a standard conductivity-temperature-depth (CTD) rosette system. During the 2015 cruise, an oxygen sensor (Seabird SBE43, Bellevue, WA) calibrated by Winkler titration (detection limit 0.7–2.5 μmol/kg), and a real-time STOX sensor (detection limit 10 nmol/L; Revsbech et al., 2009) were deployed on the CTD. During the 2016 cruise, only the Seabird oxygen sensor was deployed. Dissolved inorganic nitrogen species (NH_4^+, NO_2^-, and NO_3^-) were measured onboard: NH_4^+ was measured fluorometrically by reaction with orthophthaldialdehyde (Holmes et al., 1999); NO_2^- was measured using a colorimetric method (Hansen & Koroleff, 1999), and NO_3^- + NO_2^- was measured using cadmium reduction protocols established by United Nations Educational, Scientific and Cultural Organization (1994). See Figure S1 in the supporting information for typical profiles of oxygen and inorganic nitrogen during ETSP 2015 and ETNP 2016. Physical and chemical data from the ETSP in 2013 were described previously (Ji et al., 2015).

2.2. N_2O Production Rate Measurements

Incubation experiments to measure N_2O production using ^{15}N tracers were targeted at depths with water column features including the surface mixed layer, the base of the euphotic layer, local [NO_2^-] maxima,

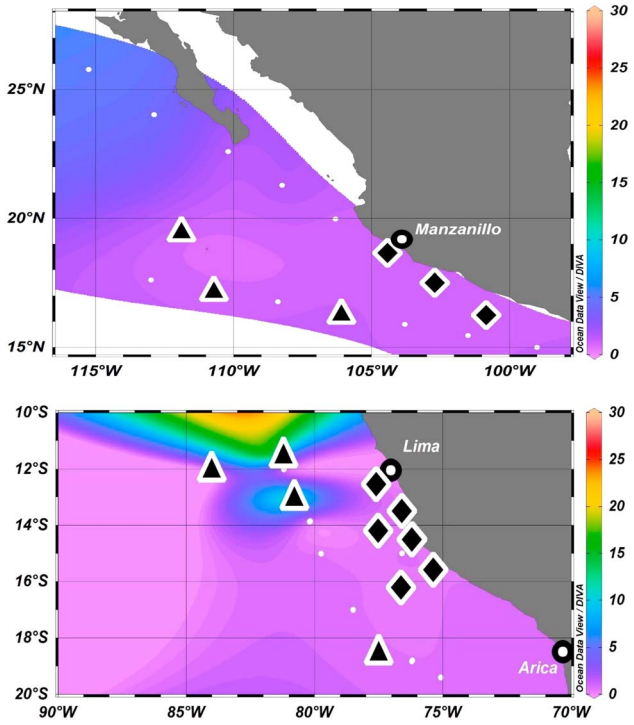

Figure 2. Sampling locations during cruises in 2016 Eastern Tropical North Pacific (upper panel) and 2015 Eastern Tropical South Pacific (lower panel). Comprehensive measurements of nitrous oxide production were performed at stations representing coastal environment (diamonds) and open ocean environment (triangles). High-resolution oxygen profiles were obtained at both comprehensive stations and transect stations (dots). Color map shows minimum dissolved oxygen concentration (μmol/L) within the upper 1,000-m water column.

sharp oxygen gradients (oxycline), and oxic-anoxic interfaces. Seawater was sampled from 12-L Niskin bottles into the bottom of acid washed, 60-ml glass serum bottles (Catalog# 223745, Wheaton, USA), and then allowed to overflow 2 to 3 times the volume before sealing the bottles with butyl septa and aluminum rings. To facilitate tracer addition, as well as compensating for oxygen contamination from air, helium headspace (3 ml) was created. Three suites of ^{15}N tracer solutions ($^{15}NH_4^+$ plus $^{14}NO_2^-$, $^{15}NO_2^-$ plus $^{14}NH_4^+$, $^{15}NO_3^-$ plus $^{14}NH_4^-$, and $^{14}NO_2^-$) were applied to enrich $^{15}NH_4^+$, $^{15}NO_2^-$, and $^{15}NO_3^-$ to 0.2, 0.4, and 0.4 μmol/L (final concentration), respectively; and increase concentrations of $^{14}NH_4^+$, $^{14}NO_2^-$, or $^{14}NO_3^-$ by 0.2, 0.4, and 0.4 μmol/L (μM), respectively. Most of the samples had in situ concentrations of NH_4^+ below 0.02 μM (Figure S1), and thus, rates of N_2O and NO_2^- production from NH_4^+ should be treated as potential rates. Samples for incubation experiments, except for one surface sample (10 m), had in situ NO_3^- concentrations >4.6 μM; samples collected from the ODZ and outside the ODZ generally had in situ NO_2^- concentrations >1 and < 0.1 μM, respectively (see supporting information Data Set S1). Tracer solutions were made from deionized water, and were flushed with helium gas before adding 0.1 ml into each sample. Incubations lasted 12–18 hr in temperature-controlled chambers (± 2 °C of in situ temperature), during which duplicate samples were preserved every 6–9 hr (three time points in total) with 0.1-ml saturated mercuric chloride ($HgCl_2$). Dilution of ^{15}N-labeled species were considered insignificant due to short incubation time.

The effect of oxygen concentrations on N_2O production was further investigated in the top of the anoxic layer (in situ $[O_2]$ <0.1 μM verified by STOX sensor). During the 2015 ETSP cruise, the depths were 160 and 80 m at offshore and coastal stations, respectively. During the 2016 ETNP cruise, the interface was at 188 and 89 m at offshore and coastal stations, respectively. Samples were acquired using a pump profiling system equipped with a CTD package, an oxygen sensor (SBE-25, Seabird Electronics, Bellevue, WA), and a real-time STOX unit. The pump profiling system minimized oxygen contamination during sampling and allowed better representation of in situ anoxic conditions during incubation experiments. The serum bottles were filled directly from the pump outlet and sealed without a headspace with septa and aluminum rings. Then, 3.2-, 3.5-, 4.0-, 5.0-, and 8.0-ml helium headspace was created; volumes of 0.2, 0.5, 1.0, 2.0, and 5.0 ml of O_2 saturated site water (~225 μM) were injected into the incubation bottles to attain 0.3-, 0.7-, 1.4-, 2.8-, and 7-μM dissolved $[O_2]$ (calculated by assuming equilibrium between the water phase and 3.0-ml final headspace in the incubation bottles (Garcia & Gordon, 1992). The same suite of tracers as above was utilized. Incubation lasted 12–18 hr at ±2 °C of in situ temperatures, during which duplicate samples were preserved every 6–9 hr (three time points in total) with 0.1-ml saturated $HgCl_2$.

Upon return to the home laboratory, N_2O in the water and headspace was stripped from the samples and analyzed using an autosampler in line with a cryofocusing unit with helium as carrier gas and injected into a Thermo-Finnigan Delta V for N_2O concentration and isotope ratio (m/z = 44, 45, 46) measurements. N_2O concentration was calculated from the amount of N_2O detected by mass spectrometry divided by the volume of seawater in the serum bottles (calibrated as 56.5 ± 0.1 ml). N_2O production was calculated from the progressive increase in mass 45 and 46 N_2O ($^{45}N_2O$ and $^{46}N_2O$) in time course experiments.

$$R = \frac{1}{F} \times \left(\frac{d^{45}N_2O}{dt} + 2 \times \frac{d^{46}N_2O}{dt} \right) \quad (1)$$

where $d^{45}N_2O/dt$ and $d^{46}N_2O/dt$ represent the production rates of during incubation of $^{45}N_2O$ and $^{46}N_2O$. F represents the ^{15}N atom fraction in the initial substrate pool (NH_4^+, NO_2^-, and NO_3^-). Rates were considered significant if the linear regression of the time course data having $p < 0.05$ (n = 5, analysis of variance, ANOVA).

2.3. NO_2^- Production Measurements

After samples were analyzed for N_2O production, samples spiked with $^{15}NH_4^+$ were also assayed for $^{15}NO_2^-$ to determine N_2O yield during nitrification. Three milliliters of each sample was transferred using a 5-ml gas-tight glass syringe (Hamilton Co., Reno, NV, USA) from the 60-ml serum bottle to a helium-flushed 20-ml glass vial (Catalog# C4020-25, Thermo Fisher Scientific, Waltham, MA). Dissolved $^{15}NO_2^-$ was converted to N_2O using the acetic acid-treated sodium azide solution for quantitative conversion (McIlvin & Altabet, 2005). Resulting N_2O was measured on the Thermo-Finnigan Delta V for isotope ratio measurements.

2.4. Data Analysis

All data were deposited in Microsoft Excel® for statistical analysis and figure production. Oxygen profiles (1-m binned-average from the CTD data package) were computed as the 5-m moving average. The depth of the oxic-anoxic interface was determined as the depth below the oxycline at which the standard deviation of the moving-averaged oxygen concentrations became <0.1 μmol/kg.

2.5. Three-Dimensional Marine N_2O Production Simulation

The prognostic global ocean general circulation Nucleus for European Modelling of the Ocean (NEMO) v3.1 model (Madec et al., 1998) was forced by daily meteorological data from the National Centers for Environmental Prediction reanalysis. Embedded in the ocean circulation model, biogeochemistry was simulated by the PlankTOM10 model (Buitenhuis et al., 2018; Le Quéré et al., 2016). The NEMO-PlankTOM10 system has a horizontal resolution of 2° with higher resolution (up to 0.5°) in tropical and polar latitudes. There are 31 vertical levels in the entire water column and 10-m resolution in the upper 100 m. The oxygen distribution in the ocean was fixed according to the reanalysis of the World Ocean Atlas oxygen data set, which had minimum $[O_2] > 1$ μM (Bianchi et al., 2012). The export production was estimated to be 5.8 Pg C/year, consistent with recent model estimates (Bisson et al., 2018; Siegel et al., 2014). The NEMO-PlankTOM10 system simulates the rates of nitrogen remineralization and N_2O production by relating oxygen consumption and organic matter remineralization below the euphotic zone:

$$[\textit{Oxygen Consumption Rate}] = \text{respiration by the 10 model plankton functional types} \quad (2)$$
$$(\text{6 phytoplankton, 3 zooplankton, and picoheterotrophs } (\textit{Bacteria} + \textit{Archaea}))$$

$$[\textit{Nitrogen remineralization rate}] = [\textit{Oxygen Consumption Rate}] \times (\text{16 mol N}/\text{172 mol } O_2) \quad (3)$$

(Takahashi et al., 1985)

Parameterization of N_2O production was modified from previous model setup (Capelle et al., 2018; Suntharalingam et al., 2012) so as to employ in situ oxygen concentrations to compute N_2O production from nitrification and denitrification:

$$\begin{aligned} &N_2O \text{ Source} = J_1 + J_2 \\ &J_1 = [a/O_2]\ (\mu M) + b \times 0.01 \times \textit{Nitrogen remineralization rate} \\ &J_2 = \beta \times f(O_2) \times [\textit{Nitrogen remineralization rate}] \end{aligned} \quad (4)$$

The two separate terms (J_1 and J_2) represent (a) NH_4^+ oxidation to N_2O in the presence of oxygen (J_1), which is parameterized according to an empirical relationship between N_2O yield and in situ O_2 concentrations during NH_4^+ oxidation (see section 3.1 and Figure 4); and (b) the enhanced N_2O production via NO_2^- and NO_3^- reduction in OMZs (J_2). The linear scaling parameter β is derived from Suntharalingam et al. (2012), which represents increased N_2O production from denitrification in suboxic conditions, and is set at 0.215, meaning up to 0.215 mol N_2O-N is produced when 1 mol of nitrogen is remineralized. The function $f(O_2)$ accounts for the functional dependence of N_2O yield on oxygen level.

$$\begin{aligned} &f(O_2) = \exp\left(\lambda\left([O_2] - [O_{2-\text{offset}}]\right)\right) \text{ when } [O_2] > [O_{2-\text{offset}}] \\ &f(O_2) = [O_2]/[O_{2-\text{offset}}] \qquad \text{when } [O_2] < [O_{2-\text{offset}}] \end{aligned} \quad (5)$$

The $[O_{2\text{-offset}}]$ represents the oxygen concentration below which net N_2O production is reduced due to N_2O consumption by denitrification, and is set to 1 μM (Capelle et al., 2018; Dalsgaard et al., 2014). The effect of O_2

Table 1
Sensitivity Analysis of Annual Global Oceanic N_2O Production From Nitrification and Denitrification

Simulation number	Nitrification yield $J_1 = [a/[O_2]\ (\mu M) + b]$	Denitrification $f(O_2) = \exp(\lambda\ (O_2\ (\mu M) - 1)$	N_2O production from nitrification (Tg-N/year)	N_2O production from denitrification (Tg-N/year)	Annual N_2O production (Tg-N)
1	$a = 0.2$, $b = 0.08$	$\lambda = -0.1$ (*e*-folding $[O_2] = 10\ \mu M$)	2.2	0.6	2.8
2	$a = 0.07$, $b = 0.04$	$\lambda = -0.1$ (*e*-folding $[O_2] = 10\ \mu M$)	1.1	0.6	1.7
3	$a = 0.33$, $b = 0.12$	$\lambda = -0.1$ (*e*-folding $[O_2] = 10\ \mu M$)	3.3	0.6	3.9
4	$a = 0.2$, $b = 0.08$	$\lambda = -0.6667$ (*e*-folding $[O_2] = 1.5\ \mu M$)	2.2	0.1	2.3
5	$a = 0.2$, $b = 0.08$	$\lambda = -0.05$ (*e*-folding $[O_2] = 20\ \mu M$)	2.2	2.1	4.3

Note. Median production was calculated based on median parameterizations for both nitrification and denitrification (simulation 1). The uncertainties for N_2O production from nitrification and denitrification were derived from simulations 2 and 3, and simulations 4 and 5, respectively.

on N_2O production from denitrification (NO_2^- and NO_3^- reduction) was experimentally measured (see section 3.2) to determine the parameterization of λ (see section 3.3 and Table 1).

The evolution of the atmospheric N_2O partial pressure since the Industrial Revolution is parameterized as follows:

$$pN_2O_{atm} = 0.000009471353 \times Y^3 - 0.05214714 \times Y^2 + 95.68066 \times Y - 58228.41 \quad (6)$$

in which pN_2O_{atm} is in natm and Y is the decimal year (Buitenhuis et al., 2018; as corrected from Freing et al., 2009). Oceanic N_2O flux to the atmosphere (F) is computed as the product of gas transfer velocity (k) and the difference between model-derived surface ocean concentration (C_s) and equilibrium concentration (C_{eq}):

$$F = k \times (C_s - C_{eq}) \quad (7)$$

The C_{eq} is computed following the equations of N_2O solubility in seawater with in situ temperature, salinity, and pN_2O_{atm} (Weiss & Price, 1980). Daily National Centers for Environmental Prediction wind product (U) and Schmidt number for N_2O (Sc) is used to calculate the gas transfer velocity k (Wanninkhof, 1992).

$$k = 0.31U^2\ (Sc/660)^{-0.5} \quad (8)$$

Model spin-up was performed to reach steady state of N_2O concentration. Thus, water column N_2O production approximated to the oceanic flux. Statistical comparison of simulated N_2O distribution pattern both at the surface and depth were performed (Figure S2) with respect to observations compiled in the MEMENTO database (Kock & Bange, 2015).

3. Results

Rates of N_2O production from NH_4^+ oxidation (Figure 3a), NO_2^- reduction (Figure 3b), and NO_3^- reduction (Figure 3c) were higher across the oxic-anoxic interface compared to depths >100 m deeper or shallower than the interface in the Eastern North and South Pacific OMZs. Highest rates of N_2O production from NH_4^+ oxidation, NO_2^- and NO_3^- reduction were detected close to (±50 m) the oxic-anoxic interface. Rates were very low at depths ≥200 m below the oxic-anoxic interface and in the oxygenated layer ≥100 m above the interface. The rates of N_2O production from nitrification and denitrification, and their control by environmental factors are presented below.

3.1. N_2O Production in the OMZs

For N_2O production from NH_4^+ oxidation, maximum rates (up to 0.05 nmol-N·L^{-1}·day^{-1}) were detected within 100 m above the oxic-anoxic interface (Figure 3a). This depth range within 100 m above the interface generally corresponds to the oxycline and N_2O supersaturation (data not shown). In the oxygenated layer, the

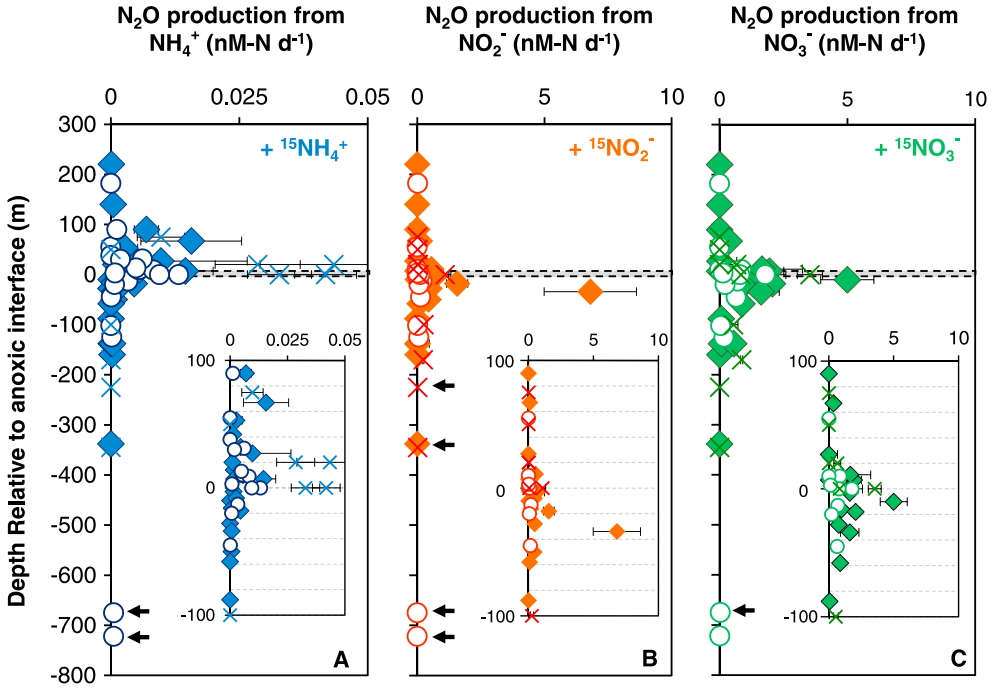

Figure 3. Rates of N_2O production from NH_4^+ oxidation (a), NO_2^- reduction (b), and NO_3^- reduction (c) at depths relative to the oxic-anoxic interface (shaded line) during cruises in 2013 Eastern Tropical South Pacific (crosses), 2015 Eastern Tropical South Pacific (filled diamonds), and 2016 Eastern Tropical North Pacific (open circles). Arrows represent significant ($p < 0.05$, see section 2) production rates at depth ≥ 200 m below oxic-anoxic interface. Inset: N_2O production from NH_4^+ oxidation (a), NO_2^- reduction (b), and NO_3^- reduction (c) within ±100 m of the oxic-anoxic interface. Error bar represents standard deviation of rates derived from a linear fit to three time points measured in duplicate ($n = 5$).

majority of the rate measurements were 0–0.02 nmol-N·L^{-1}·day^{-1}, and the rates decreased at shallower depths. In the anoxic layer below the interface, NH_4^+ oxidation is inhibited by anoxia, resulting in very low or undetectable rates of N_2O production from NH_4^+ oxidation. At deeper depths (≥200 below the oxic-anoxic interface), N_2O production rates from NH_4^+ oxidation were very slow (< 0.001 nmol-N·L^{-1}·day^{-1}). Direct measurement of N_2O yield in natural waters under a range of O_2 conditions (Figure 4) was achieved by the simultaneous measurements of N_2O and NO_2^- production from NH_4^+ oxidation. Consistent with elevated rates of N_2O production from NH_4^+ oxidation close to the oxic-anoxic interface, the N_2O yield increased nonlinearly from 0.003 to 0.06% at >50 μM O_2, to higher than 2% at <0.5 μM O_2. Particularly at O_2 concentration < 5 μM, significant increase of yield up to 2 orders of magnitude was observed with decreasing O_2 concentration. An empirical fit between N_2O yield (%) from nitrification and O_2 concentration (μM) was derived: $Yield = (0.2 \pm 0.13)/[O_2] + (0.08 \pm 0.04)$, $r^2 = 0.33$. This relationship implies that (1) the range of N_2O yield during nitrification at 0.1–300 μM O_2 concentrations is 0.04–3% and (2) outside of the OMZ at >50 μM O_2, the uncertainty range of the yield is 0.04–0.12%. Compared to previous studies relying on cultured ammonia oxidizing bacteria (AOB) for yield measurements (Goreau et al., 1980; Nevison et al., 2003), natural waters from the OMZs have tenfold to 100-fold lower yield at O_2 concentrations <10 μM (Figure 4). Within the oxycline where the O_2 concentration generally varies between 10 and 100 μM, the N_2O yield measurements of natural waters are twofold to tenfold lower than those from cultured AOB.

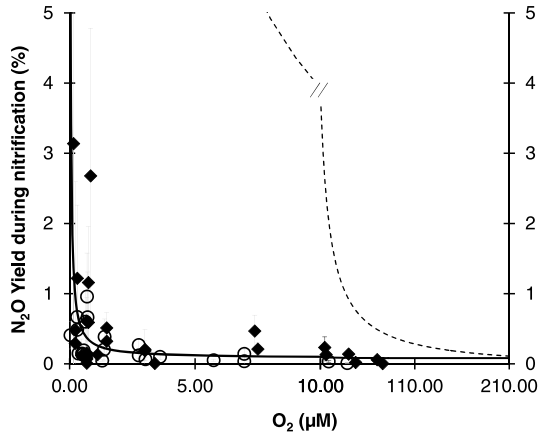

Figure 4. N_2O yield (%) during nitrification, the molar nitrogen ratio of N_2O production to NO_2^- production during NH_4^+ oxidation, measured at a range of O_2 concentrations. Data are from cruises in 2015 Eastern Tropical South Pacific (filled diamonds) and 2016 Eastern Tropical North Pacific (open circles) and compared to the N_2O yield versus oxygen relationship based on the bacterial culture work (Goreau et al., 1980; Nevison et al., 2003; dashed line) and the empirical fit in this study (solid line, *Yield* (%) = 0.2/[O_2] (μM) + 0.08).

N_2O production from both NO_2^- and NO_3^- reduction was detected in the oxycline, generally within 30 m above the oxic-anoxic interface and in the

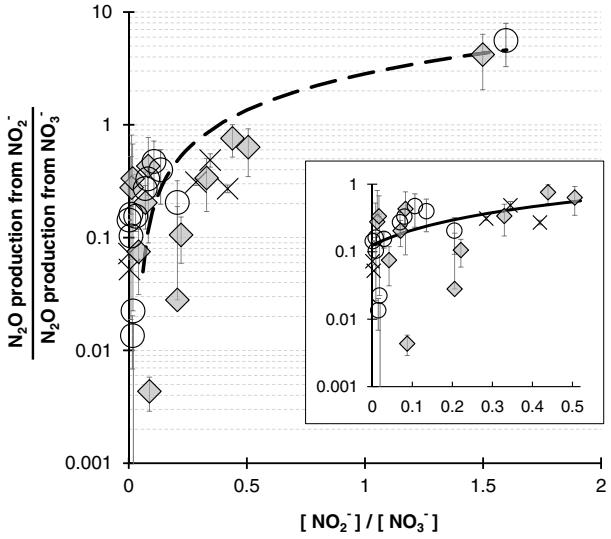

Figure 5. The ratio of N_2O production rates from NO_2^- and that from NO_3^- plotted against ratio of NO_2^- and NO_3^- concentrations during incubation experiments. Only significant production rates are plotted. Data are from cruises of 2013 Eastern Tropical South Pacific (cross), 2015 Eastern Tropical North Pacific (filled diamonds), and 2016 Eastern Tropical North Pacific (circles). Linear regressions were statistically significant for data with NO_2^- and NO_3^- concentration ratios below 0.5 (solid line, inset) and below 1.6 (dashed line). Curvature of linear regression was due to logarithmic scale on y-axis. Inset: Plotted data with NO_2^- and NO_3^- concentration ratio < 0.5.

anoxic depths (Figures 3b and 3c). Highest rates (up to 2 nmol-N·L^{-1}·day^{-1}) were detected within the oxycline and were tenfold to 100-fold higher than N_2O production from NH_4^+ oxidation. The majority of rates of NO_2^- reduction to N_2O ranged from 0 to 1.5 nmol-N·L^{-1}·day^{-1}, except for one measurement of 6.8 nmol-N·L^{-1}·day^{-1} (Figure 3b). Highest rates of N_2O production from NO_2^- and NO_3^- reduction occurred just below the oxic-anoxic interface. Both NO_2^- and NO_3^- are substrates for denitrifiers producing N_2O. However, in most paired samples, rates of N_2O production from NO_3^- reduction were twofold to sevenfold higher than N_2O production from NO_2^- reduction; the median contribution of NO_3^- reduction to total N_2O production from denitrification is 73%. The relative magnitude of the two rates may be related to the ratio of NO_2^- and NO_3^- concentrations (Figure 5). The linear regressions between the ratio of N_2O production rates from NO_2^- versus from NO_3^-, and the concentration ratio of $[NO_2^-]/[NO_3^-]$ are as follows: Within concentration ratio of 0–0.5, $y = 0.5066x + 0.0137$, $r^2 = 0.43$, $p = 0.00015$ (ANOVA, $n = 28$); within concentration ratio of 0–2.0, $y = 0.3025x + 0.0625$, $r^2 = 0.896$, $p = 1E{-}15$ (ANOVA, $n = 30$).

3.2. Effects of Oxygen on N_2O Production

The effects of elevated O_2 (0–7 μM) on N_2O production from NH_4^+ oxidation, NO_2^- reduction, and NO_3^- reduction were experimentally investigated at the oxic-anoxic interface in both coastal and offshore waters (Figure 6). Under in situ O_2 concentration (< 0.1 μM), coastal stations had higher rates of N_2O production from NH_4^+ oxidation, NO_2^- reduction, and NO_3^- reduction. An exception was that, during 2015 ETSP cruise, similar rates of NO_2^- reduction to N_2O in coastal and offshore stations were observed (0.45 nmol-N·L^{-1}·day^{-1}, Figure 6b). Highest rates of N_2O production from NH_4^+ and NO_2^- were measured under in situ O_2 concentration. These rates were significantly reduced during the course incubation experiments (within a day) in the presence of >1 μM O_2. At 7 μM O_2, rates of N_2O production from NH_4^+ and NO_2^- were reduced by 50–100% (Figures 6a and 6b). The NO_2^- data were fitted with exponential-type inhibition kinetics [$inhibition = 1 - \exp(-k \times O_2\ (\mu M))$] to derive half inhibition O_2 concentration ($C_{50} = -\ln(0.5)/k$). The C_{50} for NO_2^- reduction to N_2O in the ETSP and ETNP at both coastal and offshore stations was 1.5 ± 0.9 μM ($p = 0.01$). By contrast, increasing O_2 concentration up to 7 μM was ineffective to inhibit N_2O production from NO_3^- reduction during the 18-hr-long incubations (Figure 6c). At the coastal and offshore stations, the range of rates was 0.8–1.2 and 0–0.13 nmol-N·L^{-1}·day^{-1}, respectively. Statistical fit of the C_{50} for NO_3^- reduction to N_2O was 14 ± 4 μM ($p = 0.08$).

3.3. Global Oceanic N_2O Production

A three-dimensional ocean biogeochemical model incorporating our new data on N_2O production pathways and their sensitivities to oxygen was used to estimate marine N_2O production and oceanic efflux on the global scale. With the formulation of N_2O yield during nitrification as a function of O_2 concentration (*Yield* (%) = 0.2/[O_2] (μM) + 0.08, Figure 4), global marine N_2O efflux from nitrification was estimated as 2.2 Tg-N/year. The contribution from nitrification is small in the OMZs (< 0.05 Tg-N/year). The uncertainty of N_2O production from nitrification (1.1–3.3 Tg-N/year, simulations 2 and 3, Table 1) was derived from the parameters' uncertainties of nitrification N_2O yield (*Yield* = (0.2 ± 0.13)/[O_2] + (0.08 ± 0.04)). To estimate the range of N_2O production from denitrification, the varying sensitivities of O_2 inhibition on NO_2^- and NO_3^- reduction to N_2O were considered, which were formulated as the rates decreasing by 1/*e* (~36.8%) for 1.5 (lower boundary), 10 (median), and 20 μM (upper boundary) of O_2 increase, corresponding to $\lambda = -0.6667$, -0.1, and -0.05 for equation (6) (Table 1, simulations 1, 4, and 5). Thus, net N_2O production from denitrification ranged 0.1–2.1 Tg-N/year, with the median estimate of 0.6 Tg-N/year. Summarizing the above sensitivity analyses,

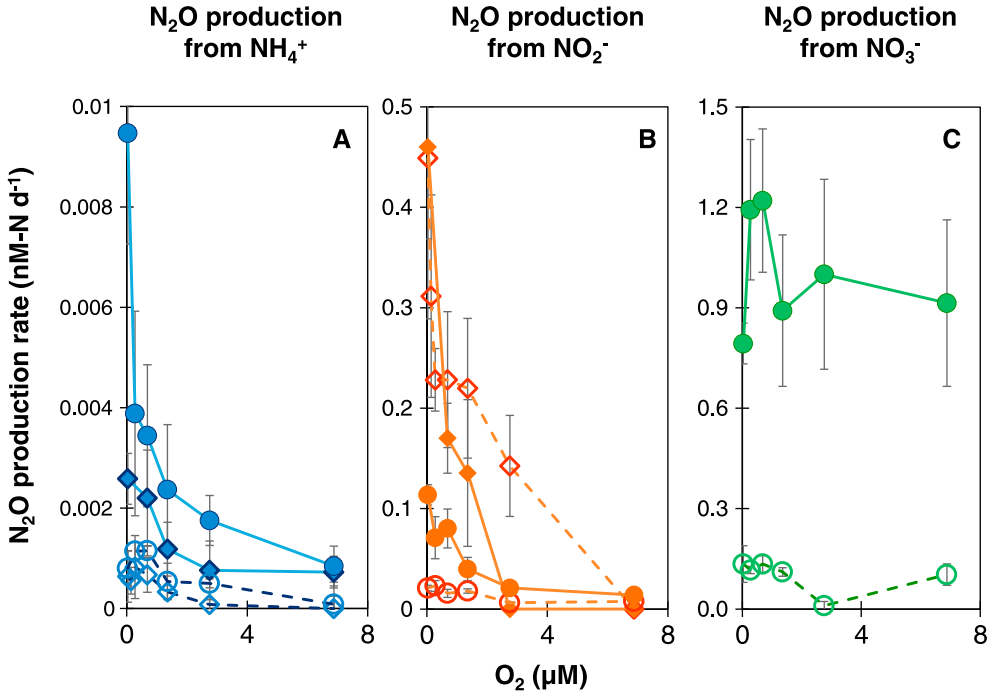

Figure 6. Rates of N_2O production from NH_4^+ oxidation (a), NO_2^- reduction (b), and NO_3^- reduction (c) under manipulated oxygen concentrations during cruises in 2015 Eastern Tropical South Pacific (diamonds) and 2016 Eastern Tropical North Pacific (circles). Measurements were performed at stations representing coastal environment (filled symbols) and open ocean environment (open symbols). The in situ oxygen concentrations at the time of sampling was <0.1 μM. Standard deviation of rates derived from a linear fit to three time points measured in duplicate (n = 5).

we estimate global oceanic N_2O efflux of 2.8 Tg-N/year (range 1.7–4.4 Tg-N/year, Table 1), with denitrification across the oxic-anoxic interface in OMZs contributing ~20% of the total fluxes.

Intense marine N_2O fluxes, 0.01–0.12 g N·m^{-2}·year^{-1} (equivalent to 0.9–9 mmol-N·m^{-2}·year^{-1}) occur in the Eastern Tropical Pacific (Figure 7). The high-latitude oceans, for example, the sub-Arctic North Atlantic and the Southern Oceans, are sites with moderate N_2O fluxes. In contrast, the fluxes were negligible in the subtropical gyres in the North and South Pacific, the North Atlantic, and South Indian Oceans.

4. Discussion

4.1. Oxidative Versus Reductive N_2O Production Pathways

The Eastern Tropical Pacific is regarded as a "hot spot" of N_2O production because of water column N_2O supersaturation near the oxic-anoxic interface. The presence of oxygenated and anoxic environments allow N_2O production via both oxidative and reductive pathways. The availability of O_2 is an important factor controlling the rate and pathways of N_2O production in OMZs (Codispoti & Christensen, 1985). The application of ^{15}N tracer incubation experiments permit the quantitative relationships between O_2 concentration and N_2O production rates and pathways.

4.1.1. N_2O Production From NH_4^+ Oxidation

The production of N_2O via NH_4^+ oxidation was identified as an important pathway in the OMZ (Cohen & Gordon, 1978). The distribution of rates in the water column of OMZ (Figure 3a) can be explained as follows: (1) In the surface waters (top 30 m), rates of NH_4^+ oxidation to NO_2^- and N_2O are minimal, mainly because NH_4^+ oxidation is suppressed by light (Ward, 2005) and phytoplankton competition for NH_4^+. (2) Within the oxycline above the ODZ, low O_2 conditions stimulated high rates of N_2O production from NH_4^+ oxidation. This is consistent with O_2 manipulation experiments showing decreased rates of N_2O production from NH_4^+ oxidation with increasing O_2 concentration (Figure 6a). (3) In the anoxic layer below the oxic-anoxic interface, NH_4^+ oxidation is inhibited, resulting in very low or undetectable rates of N_2O production from NH_4^+

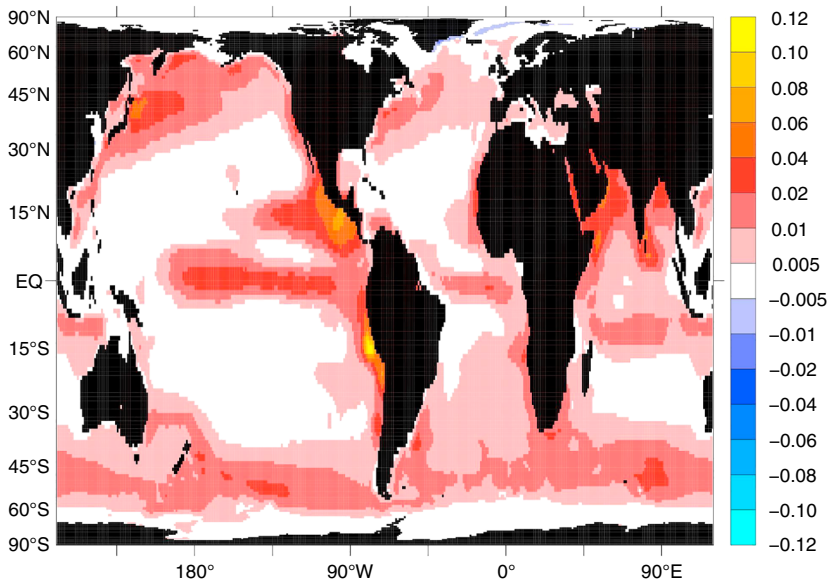

Figure 7. Global ocean N_2O flux (g N·m^{-2}·year^{-1}, color bar on the right) determined by a model simulation. Positive values indicate net flux from the ocean to the atmosphere. Simulations were performed with nitrification parameterization from this study (N_2O yield (%) = 0.2/[O_2] + 0.08), and denitrification parameterization of *e*-folding [O_2] = 10 μM. The result of global oceanic net N_2O production is 2.8 × 10^{12} g N/year.

oxidation. (4) At deeper depths below the ODZ (generally >500 m), low population density of ammonia oxidizer and low NH_4^+ availability probably limits NH_4^+ oxidation rate (Peng et al., 2016).

In oxygenated waters (>50 μM O_2), the measured N_2O yield of microbial assemblages in ETSP and ETNP (0.003–0.06%) is somewhat similar to those recently measured in cultures of marine ammonia oxidizing bacteria (Frame & Casciotti, 2010) and archaea (Löscher et al., 2012; Qin et al., 2017; Santoro et al., 2011) and is consistent with field measurements outside of OMZ (Grundle et al., 2012; Yoshida et al., 1989). Under suboxic condition ([O_2] < 5 μM), this and a previous study (Ji et al., 2015) showed N_2O yield >1%, which is much higher than any yield measured from archaea but close to bacterial yields (Frame & Casciotti, 2010; Goreau et al., 1980). The empirical relationship of N_2O yield versus O_2 concentration presented here showed that outside of OMZ, the N_2O yield is potentially twofold to tenfold lower than previously proposed (Nevison et al., 2003), which caused overestimation of global oceanic N_2O production from nitrification in some earlier studies (Bianchi et al., 2012; Suntharalingam et al., 2012). Within the OMZ, denitrification is the dominant N_2O production pathway (see section 4.1.2); thus, when estimating N_2O production via nitrification in OMZ, the error caused by overestimation of N_2O yield could be negligible.

4.1.2. N_2O Production From NO_2^- and NO_3^- Reduction

In the anoxic and the peripheral suboxic waters (generally <10 μM O_2), our ^{15}N tracer incubation experiments showed that denitrification is the dominant source of N_2O production, because rates of N_2O production from NO_2^- and NO_3^- reduction were tenfold to 100-fold higher than N_2O production from NH_4^+ oxidation. Similarly, using N_2O natural abundance isotopes, a recent study concluded that incomplete denitrification caused N_2O supersaturation in the Peruvian OMZ (Bourbonnais et al., 2017). Highest rates of N_2O production from NO_2^- and NO_3^- reduction occurred just below the oxic-anoxic interface, where O_2 inhibition of denitrification is relieved and availability of organic matter promotes denitrification. Rates of N_2O production from NO_2^- and NO_3^- reduction were higher at the coastal stations than at the offshore stations (Figure 6). This was likely due to higher organic matter content in the coastal waters resulting from higher particle flux, stimulating the growth of denitrifiers and thus denitrification (Babbin et al., 2014; Ward et al., 2008). Both NO_2^- and NO_3^- are substrates for denitrifiers producing N_2O. The ratio of rates of the two production pathways is apparently related to the ratio of NO_2^- and NO_3^- concentrations (Figure 5). Therefore, high NO_3^- availability in the water column (Figure S1) probably resulted in higher N_2O production rates from NO_3^- than from NO_2^-. Furthermore, production of N_2O from NO_3^- reduction is a series of enzymatic processes, with NO_2^-

as an intermediate, occurring inside denitrifying cells. The exchange of NO_2^- across cell membranes appears to be limited; and the coupling of NO_3^- reduction by denitrifiers and NO_2^- reduction by nitrifiers seems unlikely (Ji et al., 2015; Trimmer et al., 2016). The reduction of NO_3^- to NO_2^- (0–20 nM-N/day, data not shown) could lower the ^{15}N fraction of NO_2^- (0.4 μM added) by ~ 5%, which has minimal effect on rate calculation for N_2O production from NO_2^-. The production of N_2O from NO_2^- reduction, particularly in oxygenated waters, can be attributed to nitrifier denitrification. Rates of NO_2^- reduction to N_2O measured above the oxic-anoxic interface were 0–0.5 nmol-N·L^{-1}·day^{-1}, similar to rates measured in the peripheral suboxic waters in the ETNP (Trimmer et al., 2016).

Quantitative relationships between O_2 concentration and rates of N_2O production from NO_2^- and NO_3^- reduction can be described with half inhibition O_2 concentration (C_{50}). The C_{50} for NO_2^- reduction to N_2O in this study (0.6–2.4 μM) is somewhat higher than previously reported in the ETSP (C_{50} = 0.30 ± 0.14 μM; Dalsgaard et al., 2014). By contrast, the C_{50} for NO_3^- reduction to N_2O is tenfold higher (14 ± 4 μM). Although N_2O production from NO_3^- reduction at >7 μM O_2 was not tested, rates are expected to decrease at higher O_2 concentrations. In the stepwise denitrification pathway, the enzymes nitrate reductase and nitrite reductase are progressively less oxygen tolerant (Körner & Zumft, 1989). Thus, O_2 inhibition of denitrifying enzymes should render denitrification as an insignificant pathway in oxygenated waters outside of OMZ.

4.2. Model Evaluation for Global Oceanic N_2O Flux

With the new quantitative relationships of oxygen and N_2O production from nitrification and denitrification, and sensitivity analyses of nitrification and denitrification parameters, we estimate global oceanic N_2O efflux of 1.7–4.4 Tg-N/year. Production of N_2O outside of OMZs is attributed to nitrification, and denitrification is the dominant pathway in the OMZ. As denitrification in the OMZs contributes 20% of total oceanic fluxes, denitrification should be regarded as a net N_2O production pathway on a global perspective. Occupying <1% of global ocean volume, the OMZs of the Eastern Tropical Pacific had intense N_2O fluxes, equivalent to 0.9–9 mmol-N·m^{-2}·$year^{-1}$, which is within the range of previous flux estimates of 0–13 mmol-N·m^{-2}·$year^{-1}$ in the ETSP and ETNP (Charpentier et al., 2010; Cohen & Gordon, 1978). The production of N_2O parameterized in this study depends fundamentally on export and remineralization; therefore, the lower export production of this model (~ 6 Pg C/year) resulted lower N_2O production compared to previous studies (Battaglia & Joos, 2018; Bianchi et al., 2012; Suntharalingam et al., 2012). Statistical analysis shows that our median estimate of annual global production, 2.8 Tg-N/year best reproduces the water column and surface N_2O distribution that are currently available (Figure S2). The oxygen-dependent N_2O production rates presented here could be implemented into higher-resolution models in future studies constraining highly variable N_2O fluxes in hypoxic coastal zones (Arevalo-Martinez et al., 2015; Capelle et al., 2018). This study suggests 15% of the global N_2O emission from oceanic contribution, which is lower than Intergovernmental Panel on Climate Change's estimate of 21% (Ciais et al., 2013). Thus, the global N_2O budget could have a greater contribution from anthropogenic activities on land and coastal environments to global N_2O emissions.

The increased N_2O production rates at low-oxygen condition suggests that the ongoing ocean deoxygenation (thickening and horizontal expansion of ODZs, as well as shoaling of the upper oxycline; Stramma et al. 2008) could possibly increase future marine N_2O efflux from the OMZs (Codispoti, 2010). By the end of the 21st century, it is predicted that the Pacific Ocean will increase the OMZ volume up to 10% (Cabré et al., 2015), which will likely result in larger volume of suboxic water for net N_2O production from denitrification. Shoaling of the oxycline allows more rapid exchange between N_2O-supersaturated water and the atmosphere. It is still an open question whether the global oceanic N_2O flux will increase with the ongoing ocean warming. On one hand, warming of the surface ocean lowers N_2O solubility, leading to less N_2O retained in seawater during production and thus to increased oceanic N_2O emissions. On the other hand, the global oceanic primary production would decrease and cause lower water column remineralization and thus lower N_2O production (Landolfi et al., 2017; Martinez-Rey et al., 2015). Experimental approaches to quantify the effect of organic matter availability on N_2O production rates and pathways could facilitate predicting future oceanic N_2O emissions.

5. Conclusion

In the vicinity of water column oxic-anoxic interface within the OMZs of the Eastern Tropical Pacific, active N_2O production was measured via oxidative (NH_4^+ oxidation) and reductive pathways (NO_2^- and NO_3^- reduction). Production of N_2O from NH_4^+ oxidation occurred in the oxygenated waters, with higher rates at lower in situ oxygen concentrations. The N_2O yield during nitrification increases with decreasing oxygen concentrations; and the field measurements of N_2O yield were much lower (by twofold to tenfold) than those from culture experiments. Reduction of NO_2^- and NO_3^- to N_2O mainly occurred in the anoxic layer and suboxic zones ($[O_2] < 5$ μM) above the anoxic layer. Production of N_2O via the reductive pathways had much higher rates than that of oxidative pathway. Increasing oxygen concentrations (up to 7 μM) significantly inhibited NO_2^- reduction to N_2O; however, NO_3^- reduction to N_2O was not effectively inhibited. The relative abundance of water column NO_3^- and NO_2^- positively correlated with relative rates of N_2O production from respective substrates. In all, denitrification, particularly NO_3^- reduction is the dominating N_2O production pathway in the OMZ and adjacent suboxic waters.

We quantified the effects of oxygen concentration on N_2O production from both oxidative and reductive pathways, and implemented into a global ocean model and estimated global oceanic N_2O flux of 1.7–4.4 Tg-N/year. Although OMZs occupy a small fraction of ocean volume, high rates of N_2O production from denitrification result in OMZs contributed 20% of oceanic N_2O source. Thus, denitrification should be viewed as a net N_2O production pathway on a global perspective.

Acknowledgments
The authors would like to thank B. Widner and P. Bernhardt for providing seawater nutrient analysis; G. Alarcón for the PPS operations and the STOX sensor data on R/V *Atlantis*; M. Blum for the PPS operations on R/V *Ronald H. Brown*; and M. Mulholland as chief scientist on R/V *Atlantis* and *Ronald H. Brown*. During laboratory analysis, S. Oleynik provided valuable assistance. This research was supported by U.S.-NSF grants OCE-1029951 to B. B. Ward and OCE-1356043 to A. Jayakumar, and M. Mulholland. Erik Buitenhuis and Parvadha Suntharalingam acknowledge funding from the European Union's Horizon 2020 research and innovation programme under grant agreement 641816 Coordinated Research in Earth Systems and Climate: Experiments, kNowledge, Dissemination and Outreach (CRESCENDO). The authors declare no competing financial interests. The manuscript is prepared to comply with AGU data policy. The data reported in this study can be found in supporting information Data Set S1.

References

Arevalo-Martinez, D. L., Kock, A., Loscher, C. R., Schmitz, R. A., & Bange, H. W. (2015). Massive nitrous oxide emissions from the tropical South Pacific Ocean. *Nature Geoscience*, *8*(7), 530–533. https://doi.org/10.1038/ngeo2469

Babbin, A. R., Bianchi, D., Jayakumar, A., & Ward, B. B. (2015). Rapid nitrous oxide cycling in the suboxic ocean. *Science*, *348*(6239), 1127–1129. https://doi.org/10.1126/science.aaa8380

Babbin, A. R., Keil, R. G., Devol, A. H., & Ward, B. B. (2014). Organic matter stoichiometry, flux, and oxygen control nitrogen loss in the ocean. *Science*, *344*(6182), 406–408. https://doi.org/10.1126/science.1248364

Battaglia, G., & Joos, F. (2018). Marine N_2O emissions from nitrification and denitrification constrained by modern observations and projected in multimillennial global warming simulations. *Global Biogeochemical Cycles*, *32*, 92–121. https://doi.org/10.1002/2017GB005671

Bianchi, D., Dunne, J. P., Sarmiento, J. L., & Galbraith, E. D. (2012). Data-based estimates of suboxia, denitrification, and N_2O production in the ocean and their sensitivities to dissolved O_2. *Global Biogeochemical Cycles*, *26*, GB2009. https://doi.org/10.1029/2011GB004209

Bisson, K. M., Siegel, D. A., DeVries, T., Cael, B. B., & Buesseler, K. O. (2018). How dataset characteristics influence ocean carbon export models. *Global Biogeochemical Cycles*, *32*, 1312–1328. https://doi.org/10.1029/2018GB005934

Blasing, T. J. (2016). Recent greenhouse gas concentrations. Environmental System Science Data Infrastructure for a Virtual Ecosystem; Carbon Dioxide Information Analysis Center (CDIAC), Oak Ridge National Laboratory (ORNL), Oak Ridge, TN. https://doi.org/10.3334/CDIAC/atg.032

Bourbonnais, A., Letscher, R. T., Bange, H. W., Échevin, V., Larkum, J., Mohn, J., et al. (2017). N_2O production and consumption from stable isotopic and concentration data in the peruvian coastal upwelling system. *Global Biogeochemical Cycles*, *31*, 678–698. https://doi.org/10.1002/2016GB005567

Buitenhuis, E. T., Suntharalingam, P., & Le Quéré, C. (2018). Constraints on global oceanic emissions of N_2O from observations and models. *Biogeosciences*, *15*(7), 2161–2175. https://doi.org/10.5194/bg-15-2161-2018

Cabré, A., Marinov, I., Bernardello, R., & Bianchi, D. (2015). Oxygen minimum zones in the tropical Pacific across CMIP5 models: Mean state differences and climate change trends. *Biogeosciences*, *12*(18), 5429–5454. https://doi.org/10.5194/bg-12-5429-2015

Capelle, D. W., Hawley, A. K., Hallam, S. J., & Tortell, P. D. (2018). A multi-year time-series of N_2O dynamics in a seasonally anoxic fjord: Saanich inlet, British Columbia. *Limnology and Oceanography*, *63*(2), 524–539. https://doi.org/10.1002/lno.10645

Charpentier, J., Farías, L., & Pizarro, O. (2010). Nitrous oxide fluxes in the central and eastern South Pacific. *Global Biogeochemical Cycles*, *24*, GB3011. https://doi.org/10.1029/2008GB003388

Ciais, P., Sabine, C., Bala, G., Bopp, L., Brovkin, V., Canadell, J., Chhabra, A., et al. (2013). *Carbon and other biogeochemical cycles* (pp. 465–570). Cambridge, United Kingdom and New York: Cambridge Univ. Press. https://doi.org/10.1017/CBO9781107415324.015

Codispoti, L. A. (2010). Interesting times for marine N_2O. *Science*, *327*(5971), 1339–1340. https://doi.org/10.1126/science.1184945

Codispoti, L. A., Brandes, J. A., Christensen, J. P., Devol, A. H., Naqvi, S. W. A., Paerl, H. W., & Yoshinari, T. (2001). The oceanic fixed nitrogen and nitrous oxide budgets: Moving targets as we enter the anthropocene? *Scientia Marina*, *65*(S2), 85–105. https://doi.org/10.3989/scimar.2001.65s285

Codispoti, L. A., & Christensen, J. P. (1985). Nitrification, denitrification and nitrous oxide cycling in the eastern tropical South Pacific Ocean. *Marine Chemistry*, *16*(4), 277–300. https://doi.org/10.1016/0304-4203(85)90051-9

Cohen, Y., & Gordon, L. I. (1978). Nitrous oxide in the oxygen minimum of the eastern tropical North Pacific: Evidence for its consumption during denitrification and possible mechanisms for its production. *Deep-Sea Research*, *25*(6), 509–524. https://doi.org/10.1016/0146-6291(78)90640-9

Dalsgaard, T., Stewart, F. J., Thamdrup, B., De Brabandere, L., Revsbech, N. P., Ulloa, O., et al. (2014). Oxygen at nanomolar levels reversibly suppresses process rates and gene expression in anammox and denitrification in the oxygen minimum zone off northern Chile. *MBio*, *5*(6). https://doi.org/10.1128/mBio.01966-14

Elkins, J. W., Wofsy, S. C., Mcelroy, M. B., Kolb, C. E., & Kaplan, W. A. (1978). Aquatic sources and sinks for nitrous oxide. *Nature*, *275*(5681), 602–606. https://doi.org/10.1038/275602a0

Frame, C. H., & Casciotti, K. L. (2010). Biogeochemical controls and isotopic signatures of nitrous oxide production by a marine ammonia-oxidizing bacterium. *Biogeosciences*, *7*(9), 2695–2709. https://doi.org/10.5194/bg-7-2695-2010

Freing, A., Wallace, D. W., & Bange, H. W. (2012). Global oceanic production of nitrous oxide. *Philosophical Transactions of the Royal Society of London. Series B, Biological Sciences*, *367*(1593), 1245–1255. https://doi.org/10.1098/rstb.2011.0360

Freing, A., Wallace, D. W. R., Tanhua, T., Walter, S., & Bange, H. W. (2009). North Atlantic production of nitrous oxide in the context of changing atmospheric levels. *Global Biogeochemical Cycles*, *23*, GB4015. https://doi.org/10.1029/2009GB003472

Garcia, H. E., & Gordon, L. I. (1992). Oxygen solubility in seawater: Better fitting equations. *Limnology and Oceanography*, *37*(6), 1307–1312. https://doi.org/10.4319/lo.1992.37.6.1307

Goreau, T. J., Kaplan, W. A., Wofsy, S. C., McElroy, M. B., Valois, F. W., & Watson, S. W. (1980). Production of NO_2^- and N_2O by nitrifying bacteria at reduced concentrations of oxygen. *Applied and Environmental Microbiology*, *40*(3), 526–532.

Grundle, D. S., Maranger, R., & Juniper, S. K. (2012). Upper water column nitrous oxide distributions in the northeast Subarctic Pacific Ocean. *Atmosphere-Ocean*, *50*(4), 475–486. https://doi.org/10.1080/07055900.2012.727779

Hansen, H. P., & Koroleff, F. (1999). *Determination of nutrients*. Weinheim, Germany: Wiley-VCH Verlag GmbH.

Holmes, R. M., Aminot, A., Kerouel, R., Hooker, B. A., & Peterson, B. J. (1999). A simple and precise method for measuring ammonium in marine and freshwater ecosystems. *Canadian Journal of Fisheries and Aquatic Sciences*, *56*(10), 1801–1808. https://doi.org/10.1139/f99-128

Ji, Q., Babbin, A. R., Jayakumar, A., Oleynik, S., & Ward, B. B. (2015). Nitrous oxide production by nitrification and denitrification in the eastern tropical South Pacific oxygen minimum zone. *Geophysical Research Letters*, *42*, 10,755–10,764. https://doi.org/10.1002/2015GL066853

Kock, A., & Bange, H. W. (2015). Counting the ocean's greenhouse gas emissions. *Eos*, *96*, 10–13. https://doi.org/10.1029/2015EO023665

Körner, H., & Zumft, W. G. (1989). Expression of denitrification enzymes in response to the dissolved oxygen level and respiratory substrate in continuous culture of *Pseudomonas stutzeri*. *Applied and Environmental Microbiology*, *55*(7), 1670–1676.

Landolfi, A., Somes, C. J., Koeve, W., Zamora, L. M., & Oschlies, A. (2017). Oceanic nitrogen cycling and n2o flux perturbations in the anthropocene. *Global Biogeochemical Cycles*, *31*, 1236–1255. https://doi.org/10.1002/2017GB005633

Law, C. S., & Owens, N. J. P. (1990). Significant flux of atmospheric nitrous oxide from the northwest Indian Ocean. *Nature*, *346*(6287), 826–828. https://doi.org/10.1038/346826a0

Le Quéré, C., Buitenhuis, E. T., Moriarty, R., Alvain, S., Aumont, O., Bopp, L., et al. (2016). Role of zooplankton dynamics for southern ocean phytoplankton biomass and global biogeochemical cycles. *Biogeosciences*, *13*(14), 4111–4133. https://doi.org/10.5194/bg-13-4111-2016

Löscher, C. R., Kock, A., Könneke, M., LaRoche, J., Bange, H. W., & Schmitz, R. A. (2012). Production of oceanic nitrous oxide by ammonia-oxidizing archaea. *Biogeosciences*, *9*(7), 2419–2429. https://doi.org/10.5194/bg-9-2419-2012

Madec, G., Delecluse, P., Imbard, M., & Lévy, C. (1998), Opa 8.1 ocean general circulation model reference manual, notes pole model, edited by I. P. S. L. d. S. d. l. E. Global, p. 91, Laboratoire d'Océanographie DYnamique et de Climatologie.

Martinez-Rey, J., Bopp, L., Gehlen, M., Tagliabue, A., & Gruber, N. (2015). Projections of oceanic N_2O emissions in the 21st century using the IPSL Earth system model. *Biogeosciences*, *12*(13), 4133–4148. https://doi.org/10.5194/bg-12-4133-2015

McIlvin, M. R., & Altabet, M. A. (2005). Chemical conversion of nitrate and nitrite to nitrous oxide for nitrogen and oxygen isotopic analysis in freshwater and seawater. *Analytical Chemistry*, *77*(17), 5589–5595. https://doi.org/10.1021/ac050528s

Nevison, C., Butler, J. H., & Elkins, J. W. (2003). Global distribution of N_2O and the δN_2O-AOU yield in the subsurface ocean. *Global Biogeochemical Cycles*, *17*(4), 1119. https://doi.org/10.1029/2003GB002068

Peng, X., Fuchsman, C. A., Jayakumar, A., Warner, M. J., Devol, A. H., & Ward, B. B. (2016). Revisiting nitrification in the eastern tropical South Pacific: A focus on controls. *Journal of Geophysical Research: Oceans*, *121*, 1667–1684. https://doi.org/10.1002/2015JC011455

Poth, M., & Focht, D. D. (1985). ^{15}N kinetic analysis of N_2O production by *Nitrosomonas europaea*: An examination of nitrifier denitrification. *Applied and Environmental Microbiology*, *49*(5), 1134–1141.

Prather, M. J., Holmes, C. D., & Hsu, J. (2012). Reactive greenhouse gas scenarios: Systematic exploration of uncertainties and the role of atmospheric chemistry. *Geophysical Research Letters*, *39*, L09803. https://doi.org/10.1029/2012GL051440

Qin, W., Meinhardt, K. A., Moffett, J. W., Devol, A. H., Virginia Armbrust, E., Ingalls, A. E., & Stahl, D. A. (2017). Influence of oxygen availability on the activities of ammonia-oxidizing archaea. *Environmental Microbiology Reports*, *9*(3), 250–256. https://doi.org/10.1111/1758-2229.12525

Ravishankara, A., Daniel, J. S., & Portmann, R. W. (2009). Nitrous oxide (N_2O): The dominant ozone-depleting substance emitted in the 21st century. *Science*, *326*(5949), 123–125. https://doi.org/10.1126/science.1176985

Revsbech, N. P., Larsen, L. H., Gundersen, J., Dalsgaard, T., Ulloa, O., & Thamdrup, B. (2009). Determination of ultra-low oxygen concentrations in oxygen minimum zones by the STOX sensor. *Limnology and Oceanography: Methods*, *7*(5), 371–381. https://doi.org/10.4319/lom.2009.7.371

Santoro, A. E., Buchwald, C., McIlvin, M. R., & Casciotti, K. L. (2011). Isotopic signature of N_2O produced by marine ammonia-oxidizing archaea. *Science*, *333*(6047), 1282–1285. https://doi.org/10.1126/science.1208239

Siegel, D. A., Buesseler, K. O., Doney, S. C., Sailley, S. F., Behrenfeld, M. J., & Boyd, P. W. (2014). Global assessment of ocean carbon export by combining satellite observations and food-web models. *Global Biogeochemical Cycles*, *28*, 181–196. https://doi.org/10.1002/2013GB004743

Stramma, L., Johnson, G. C., Sprintall, J., & Mohrholz, V. (2008). Expanding oxygen-minimum zones in the tropical oceans. *Science*, *320*(5876), 655–658. https://doi.org/10.1126/science.1153847

Suntharalingam, P., Buitenhuis, E., Le Quéré, C., Dentener, F., Nevison, C., Butler, J. H., et al. (2012). Quantifying the impact of anthropogenic nitrogen deposition on oceanic nitrous oxide. *Geophysical Research Letters*, *39*, L07605. https://doi.org/10.1029/2011GL050778

Takahashi, T., Broecker, W. S., & Langer, S. (1985). Redfield ratio based on chemical data from isopycnal surfaces. *Journal of Geophysical Research*, *90*(C4), 6907–6924. https://doi.org/10.1029/JC090iC04p06907

Trimmer, M., Chronopoulou, P.-M., Maanoja, S. T., Upstill-Goddard, R. C., Kitidis, V., & Purdy, K. J. (2016). Nitrous oxide as a function of oxygen and archaeal gene abundance in the north Pacific. *Nature Communications*, *7*(1), 13451. https://doi.org/10.1038/ncomms13451

United Nations Educational, Scientific and Cultural Organization (1994). Protocols for the joint global ocean flux study (JGOFS) core measurements, edited by I. O. Commission, United Nations Educational, Scientific and Cultural Organization.

Wanninkhof, R. (1992). Relationship between wind speed and gas exchange over the ocean. *Journal of Geophysical Research*, *97*(C5), 7373–7382. https://doi.org/10.1029/92JC00188

Ward, B. B. (2005). Temporal variability in nitrification rates and related biogeochemical factors in Monterey Bay, California, USA. *Marine Ecology Progress Series*, *292*, 97–109. https://doi.org/10.3354/meps292097

Ward, B. B., Tuit, C. B., Jayakumar, A., Rich, J. J., Moffett, J., & Naqvi, S. W. A. (2008). Organic carbon, and not copper, controls denitrification in oxygen minimum zones of the ocean. *Deep-Sea Research Part I: Oceanographic Research Papers*, *55*(12), 1672–1683. https://doi.org/10.1016/j.dsr.2008.07.005

Weiss, R. F., & Price, B. A. (1980). Nitrous oxide solubility in water and seawater. *Marine Chemistry*, *8*(4), 347–359. https://doi.org/10.1016/0304-4203(80)90024-9

Wilson, S. T., del Valle, D. A., Segura-Noguera, M., & Karl, D. M. (2014). A role for nitrite in the production of nitrous oxide in the lower euphotic zone of the oligotrophic North Pacific Ocean. *Deep-Sea Research Part I: Oceanographic Research Papers*, *85*, 47–55. https://doi.org/10.1016/j.dsr.2013.11.008

Yoshida, N., Morimoto, H., Hirano, M., Koike, I., Matsuo, S., Wada, E., et al. (1989). Nitrification rates and ^{15}N abundances of N_2O and NO_3^- in the western North Pacific. *Nature*, *342*(6252), 895–897. https://doi.org/10.1038/342895a0